A Research Report to AFOSR/AOARD

(Project Number: FA2386-11-1-4038)

CONSTITUTIVE ANALYSIS OF HIGH-TEMPERATURE DEFORMATION BEHAVIOR OF FINE- AND COARSE-GRAINED TWO-PHASE TITANIUM ALLOYS

by

Taekyung Lee[1] and Chong Soo Lee

Department of Materials Science and Engineering,

Pohang University of Science and Technology,

Pohang 790-784, Republic of Korea

August 15, 2012

Report Documentation Page

Form Approved
OMB No. 0704-0188

1. REPORT DATE	2. REPORT TYPE	3. DATES COVERED
23 AUG 2012	**Final**	**21-07-2011 to 20-07-2012**

4. TITLE AND SUBTITLE
Constitutive Analysis of High-Temperature Deformation Behavior of Fine- and Coarse-Grained Two-Phase Titanium alloys

5a. CONTRACT NUMBER
FA23861114038

5b. GRANT NUMBER

5c. PROGRAM ELEMENT NUMBER

6. AUTHOR(S)
Chong Soo Lee

5d. PROJECT NUMBER

5e. TASK NUMBER

5f. WORK UNIT NUMBER

7. PERFORMING ORGANIZATION NAME(S) AND ADDRESS(ES)
Pohang University of Science and Technology,San 31, Hyoja-dong, Nam-gu,Pohang 790-784,Korea (South),KR,790784

8. PERFORMING ORGANIZATION REPORT NUMBER
N/A

9. SPONSORING/MONITORING AGENCY NAME(S) AND ADDRESS(ES)
AOARD, UNIT 45002, APO, AP, 96338-5002

10. SPONSOR/MONITOR'S ACRONYM(S)
AOARD

11. SPONSOR/MONITOR'S REPORT NUMBER(S)
AOARD-114038

12. DISTRIBUTION/AVAILABILITY STATEMENT
Approved for public release; distribution unlimited

13. SUPPLEMENTARY NOTES

14. ABSTRACT

The present work investigated high-temperature deformation behavior (flow curve, strain rate sensitivity, deformation mode) in Ti-5Al-4V alloys using both Strain Rate Jump (SRJT) and Load Relaxation (LRT) Tests. The disparity in high temperature plasticity was observed by directly comparing two groups of results, and elucidated on the basis of microstructural evolution and semi-constitutive and quantitative analysis called internal-variable analysis. Stress-strain rate plots determined from SRJT and LRT were in good agreement with theoretical predictions considering the activation of grain-matrix deformation and particle/grain-boundary sliding. The relative contribution of the two mechanisms varied with the microstructure, temperature, strain rate, which affected the flow stress and strain rate sensitivity of the Ti-6Al-4V. A clear difference in strain rate sensitivity was observed depending on the experimental method; SRJT values were higher than those from the LRT in all cases. Such a discrepancy could be attributed to a variation in pre-strain between the two methods. This variation resulted in microstructural differences, such as the fraction of alpha/beta interfaces and the misorientation of alpha grain boundaries, and hence affected the contribution of particle/grain-boundary sliding to the overall deformation.

15. SUBJECT TERMS
Grain Size Effects, Titanium Alloys, Strain Rate Effects

16. SECURITY CLASSIFICATION OF:			17. LIMITATION OF ABSTRACT	18. NUMBER OF PAGES	19a. NAME OF RESPONSIBLE PERSON
a. REPORT	b. ABSTRACT	c. THIS PAGE			
unclassified	**unclassified**	**unclassified**	**Same as Report (SAR)**	**32**	

ABSTRACT

Studies of constitutive modeling and analysis for plastic flow during high-temperature deformation have conducted widely due to the importance of designing bulk hot-working processes. The strain rate jump test (SRJT) and load relaxation test (LRT) are among the most common experimental methods used to evaluate the high-temperature deformation behavior. Despite their importance, however, the determined results appear to vary with the experimental method. Hence, the present work investigated the high-temperature deformation behavior such as a flow curve, strain rate sensitivity, and deformation mode, in Ti-6Al-4V alloys using both SRJT and LRT. The disparity in high-temperature plasticity was observed by directly comparing two groups of results, and elucidated on the basis of microstructural evolution and the semi-constitutive and quantitative analysis called the internal-variable analysis. Stress - strain rate plots determined from SRJT and LRT were in good agreement with the theoretical predictions considering the activation of grain-matrix deformation and particle/grain-boundary sliding. The relative contribution of the two mechanisms varied with the microstructure, temperature, and strain rate, which affected the flow stress and strain rate sensitivity of the Ti-6Al-4V. A clear difference in the strain rate sensitivity was observed depending on the experimental method; the SRJT values were higher than those from the LRT in all cases. Such a discrepancy could be attributed to a variation in prestrain between the two methods. This variation resulted in microstructural differences, such as the fraction of alpha/beta interfaces and the misorientation of alpha grain boundaries, and hence affected the contribution of particle/grain-boundary sliding to the overall deformation.

Contents

1. Introduction

Constitutive modeling and analysis for plastic flow at high temperature is one of major issues in materials science due to the importance of designing bulk hot-working processes. Accordingly, many works on high-temperature deformation behavior and its constitutive analysis have been performed for various structural metallic alloys [1-4]. One alloy whose behavior has been documented is Ti-6Al-4V, which is used widely in the aerospace industry due to its high strength-to-weight ratio, good formability, and superior corrosion resistance [5-7].

The strain rate sensitivity (m-value) is one of key parameters in high-temperature plastic flow and constitutive analysis, which is used for evaluating high-temperature deformation behavior of a material. For example, a material with an m-value higher than 0.3 is generally considered to possess *superplasticity* that exhibits very large tensile elongation [8]. The strain rate sensitivity is determined on the basis of the dependence of flow stress (σ) on strain rate ($\dot{\varepsilon}$), expressed as:

$$m = \partial \log \sigma / \partial \log \dot{\varepsilon}|_{\varepsilon,T} \tag{1}$$

There are two common experimental methods to determine the strain rate sensitivity: the strain rate jump test (SRJT) [9] and load relaxation test (LRT) [10]. The SRJT yields the m-value based on the logarithmic ratios of the stresses (σ) and strain rates ($\dot{\varepsilon}$) just before and after a strain rate jump, *i.e.*, $m = \log(\sigma_2/\sigma_1)/\log(\dot{\varepsilon}_2/\dot{\varepsilon}_1)$. For the LRT, the m-value is determined from the slope of a log stress - log strain rate plot.

From previous reports, the strain rate sensitivity of a given material appears to vary with the experimental method used to determine it. For example, Hedworth and Stowell [11]

determined the strain rate sensitivity of an Al-Cu eutectic alloy using both SRJT and LRT, and proposed significant differences with m-values ranging from 0.42 to 1.25 depending on the method. For Ti-6Al-4V, there also appears to be a discrepancy in the published literature. For example, Semiatin *et al.* [12] reported m ~0.75 based on SRJT data at 815°C, whereas Kim *et al.* [13] reported m ~0.35 from LRT data at the same temperature. Such significant differences can be explained in part based on variations in microstructure of the respective program materials (*e.g.*, alpha particle size) and test technique.

Although previous research has suggested that the strain rate sensitivity can be different depending on the experimental method, there appears to have been no work that directly compares data from different test methods and systematically analyzes the discrepancies in the obtained values. Moreover, semi-quantitative analyses using the internal-variable theory have for the most part only been conducted using LRT data. Hence, the present research aims at performing the internal-variable analysis on the mechanism of high-temperature deformation in Ti-6Al-4V using both SRJT and LRT methods, clarifying the specific quantitative dependence of the strain rate sensitivity on test method, and elucidating factors that influence plastic-flow phenomena on the basis of the internal-variable theory.

2. Internal-variable theory

The internal-variable theory [2] quantifies the relative contribution of grain matrix deformation (GMD) and particle/grain-boundary sliding (P/GBS) during high-temperature deformation (Fig. 1).

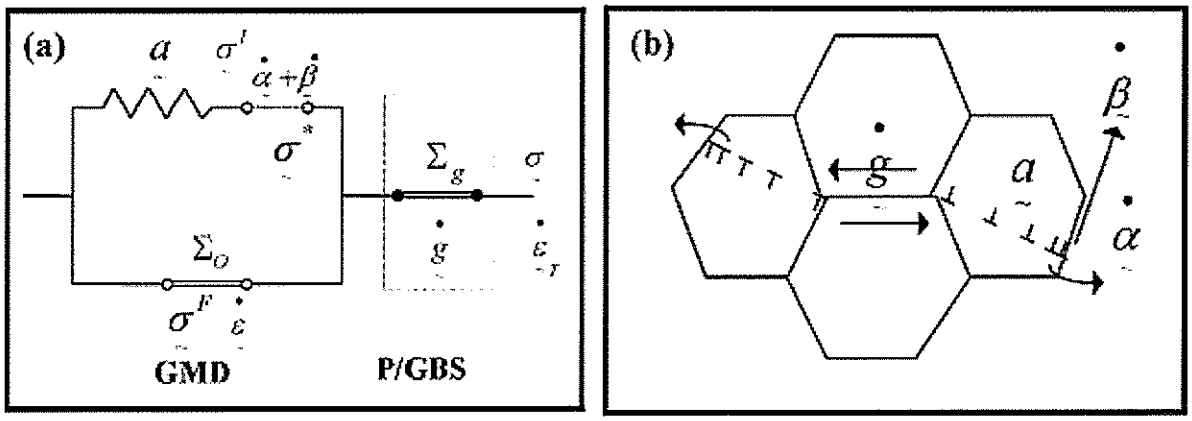

Fig. 1 (a) Rheological and (b) topological model of the internal-variable theory [2].

The kinematic relations in the theory are derived as follows:

$$\sigma = \sigma^I + \sigma^F \tag{2}$$

$$\dot{\varepsilon} = \dot{a} + \dot{\alpha} + \dot{g} \tag{3}$$

in which σ^I is the internal stress caused by long-range dislocation interactions, and σ^F is the friction stress due to short-range interactions between dislocations and the lattice. $\dot{a}$, $\dot{\alpha}$, and $\dot{g}$ denote the strain rates caused by an internal strain, non-recoverable plastic strain, and P/GBS, respectively. The terms σ^F and $\dot{a}$ are generally small enough to be neglected during nearly steady-state deformation at high temperatures, which allows the following simplified relations to be used in the present work:

$$\sigma \cong \sigma^{I} \tag{4}$$

$$\dot{\varepsilon} \cong \dot{\alpha} + \dot{g} \tag{5}$$

The parameters in Eqs. (4) and (5) are determined using the following expressions:

$$(\sigma^{*}/\sigma^{I}) = \exp\,(\dot{\alpha}^{*}/\dot{\alpha})^{p} \tag{6a}$$

$$\dot{\alpha}^{*} = \nu^{I}(\sigma^{*}/G)^{n^{I}} \exp\,(-Q^{I}/RT) \tag{6b}$$

$$(\dot{g}/\dot{g}_{0}) = \left[(\sigma - \Sigma_{g})/\Sigma_{g}\right]^{1/M_{g}} \tag{7a}$$

$$\dot{g}_{o} = \nu^{g}\left(\Sigma_{g}/\mu^{g}\right)^{n^{g}} \exp\,(-Q^{g}/RT) \tag{7b}$$

Here, σ^{*} is the internal stress for the GMD related to its conjugate reference strain rate $\dot{\alpha}^{*}$. Σ_{g} is the friction stress for the P/GBS related to its conjugate reference strain rate $\dot{g}_{0}$. ν is the jump frequency for dislocations at the grain boundaries, Q is activation energy, R is the gas constant, T is the deformation temperature, G and μ^{g} are moduli, and the other parameters are material constants.

3. Experimental procedures

3.1. Material preparation

The material used in the present investigation was Ti-6Al-4V plate with an initial thickness of 20 mm. Sections of this material were solution treated at 1050°C for 2 hours, water quenched, and then cross-rolled at 800°C to a thickness reduction of 80%, followed by water quenching. The rolling procedure consisted of 15% reduction per pass to a total reduction of 60% followed by a final pass of 20% reduction. This material is denoted as fine-particle (FP) Ti-6Al-4V. Other sections of the as-received plate were prepared using the same procedure as that employed to fabricate FP Ti-6Al-4V, but were subsequently annealed at 930°C for 5 hours to induce particle/grain growth. This latter material is denoted as coarse-particle (CP) Ti-6Al-4V.

3.2. Microstructural observation

Microstructural analysis was performed using backscattered electron (BSE) imaging in a field-emission scanning electron microscope (FE-SEM) at 15 kV and electron backscatter diffraction (EBSD) technique at 20 kV. All samples were wet-abraded with #400, #800, #1200, and #2400 SiC paper. Sections of these samples were subsequently polished using 1 μm diamond suspensions for the BSE imaging. Other sections were electro-polished at 22 V in a solution of 40 ml $HClO_4$ (60%), 245 ml 2-butoxy ethanol, and 410 ml methanol, which were used for the EBSD observation. The fraction of alpha and beta phases was determined by counting pixels in the BSE images. The average size of the alpha particles was determined by dividing the total area of alpha by the number of particles in the BSE images [14].

3.3. High-temperature experiments

SRJT and LRT were conducted at 700, 800, and 900°C. Each sample was soaked at each temperature for 10 minutes prior to commencing the tests.

3.3.1. SRJT

A tensile specimen with a gauge length, width, and thickness of 5 mm, 4 mm, and 2 mm, respectively, was used. The tests were conducted using true strain rates of 10^{-2}, 10^{-3}, and 10^{-4} s^{-1}, which were increased by 40 percent at a true strain of 0.25. To aid in the internal-variable analysis of the CP material, selected additional SRJT experiments were done for this material at 700 °C and 900 °C using strain rates of 5 x 10^{-2} s^{-1} and 5 x 10^{-3} s^{-1}. During each portion of the SRJTs, the crosshead speed v was changed continuously to maintain constant true strain rate per the following relation:

$$v = L\dot{\varepsilon} = L_0\dot{\varepsilon}\exp(\dot{\varepsilon}t) \tag{8}$$

in which L is the instantaneous gauge length at test time t, and L_0 is the initial gauge length [15].

3.3.2. LRT

A specimen with a gauge length, width, and thickness of 25 mm, 5 mm, and 2 mm, respectively, was used. Samples were pulled to a true strain of 0.05 at a strain rate of 10^{-2} s^{-1}, after which the crosshead was held fixed during the relaxation step. Stress - strain rate plots were derived from the measured data using the relations suggested by Lee and Hart [10]:

$$\sigma = P(L_0 + X - P/K)/A_0L_0 \tag{9a}$$

$$\dot{\varepsilon} = -\dot{P}/K(L_0 + X - P/K) \tag{9b}$$

$$K^{-1} = C_m + L/AE \cong C_m + L_0/A_0E \tag{9c}$$

Here, P and $\dot{P}$ denote the load and its time derivative, respectively, A_0 is the initial cross-sectional area, X is the crosshead displacement, C_m (= 1.7 x 10^{-3} mm/kN) is the elastic compliance of the machine, and E (= 114 GPa) is Young's modulus.

4. Results

4.1. Initial microstructures of investigated alloys

From BSE images, the FP condition was found to exhibit a severely distorted microstructure in which the alpha laths and beta layers were partly fragmented into small particles (Fig. 2(a)). This type of microstructural evolution is commonly found in severely deformed materials for which dynamic globularization transforms a martensitic or lamellar structure into fine and equiaxed particles. For example, an analogous microstructure was reported in cross-rolled Ti-6Al-2Sn-4Zr-2Mo-0.1Si with an initial martensitic structure [16] and caliber-rolled carbon steels which were initially composed of lamellar pearlite colonies [17]. The corresponding EBSD grain-boundary map revealed that ultrafine equiaxed grains were produced within the alpha particles.

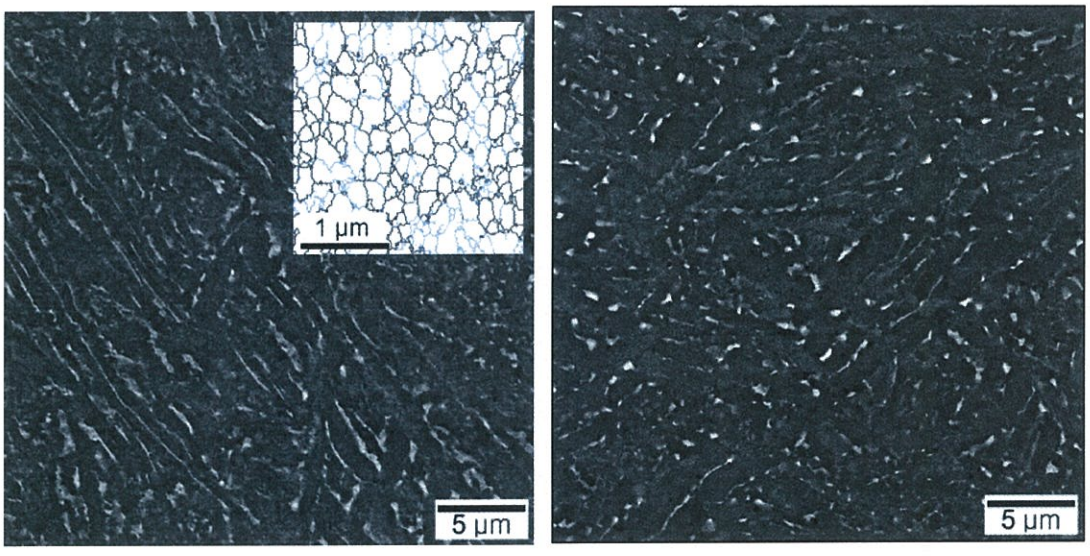

(a) (b)

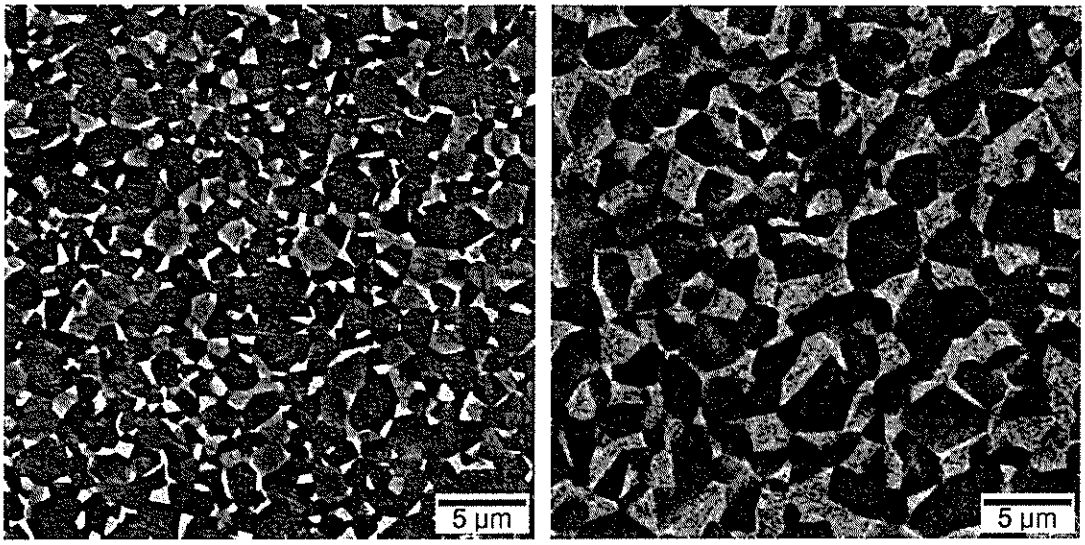

(c) (d)

Fig. 2 BSE micrographs of FP Ti-6Al-4V (a) in the initial condition and just prior to SRJT or LRT at (b) 700 °C, (c) 800 °C, or (d) 900 °C. The dark and light areas denote the alpha and beta phases, respectively. The inset image in Fig. 2(a) is an EBSD-derived map in which black and blue lines indicate high-angle ($\theta > 15°$) and low-angle ($2° < \theta < 15°$) boundaries, respectively.

The microstructures prior to SRJT and LRT (prepared by heating the FP samples for 10 minutes, followed by water quenching) (Fig. 2(b)-(d)) revealed that tests at 800°C and 900°C were conducted with a fully globularized FP sample. In contrast, beta lamellae, which were not totally fragmented, remained before commencing high-temperature tests at 700°C. Furthermore, the fraction of alpha phase decreased with increasing temperature: 94.5% at 700°C, 83.2% at 800°C, and 63.6% at 900°C.

For the CP material, samples in either the initial condition or just prior to the high-temperature deformation exhibited a microstructure consisting of coarse, equiaxed alpha particles surrounded by the beta-phase matrix (Fig. 3). The fraction of alpha phase was determined to be 89.0% at 700°C, 77.6% at 800°C, and 61.8% at 900°C. The difference in the

fraction of alpha in the FP and CP materials at a given temperature can be ascribed to experimental uncertainty in such measurements.

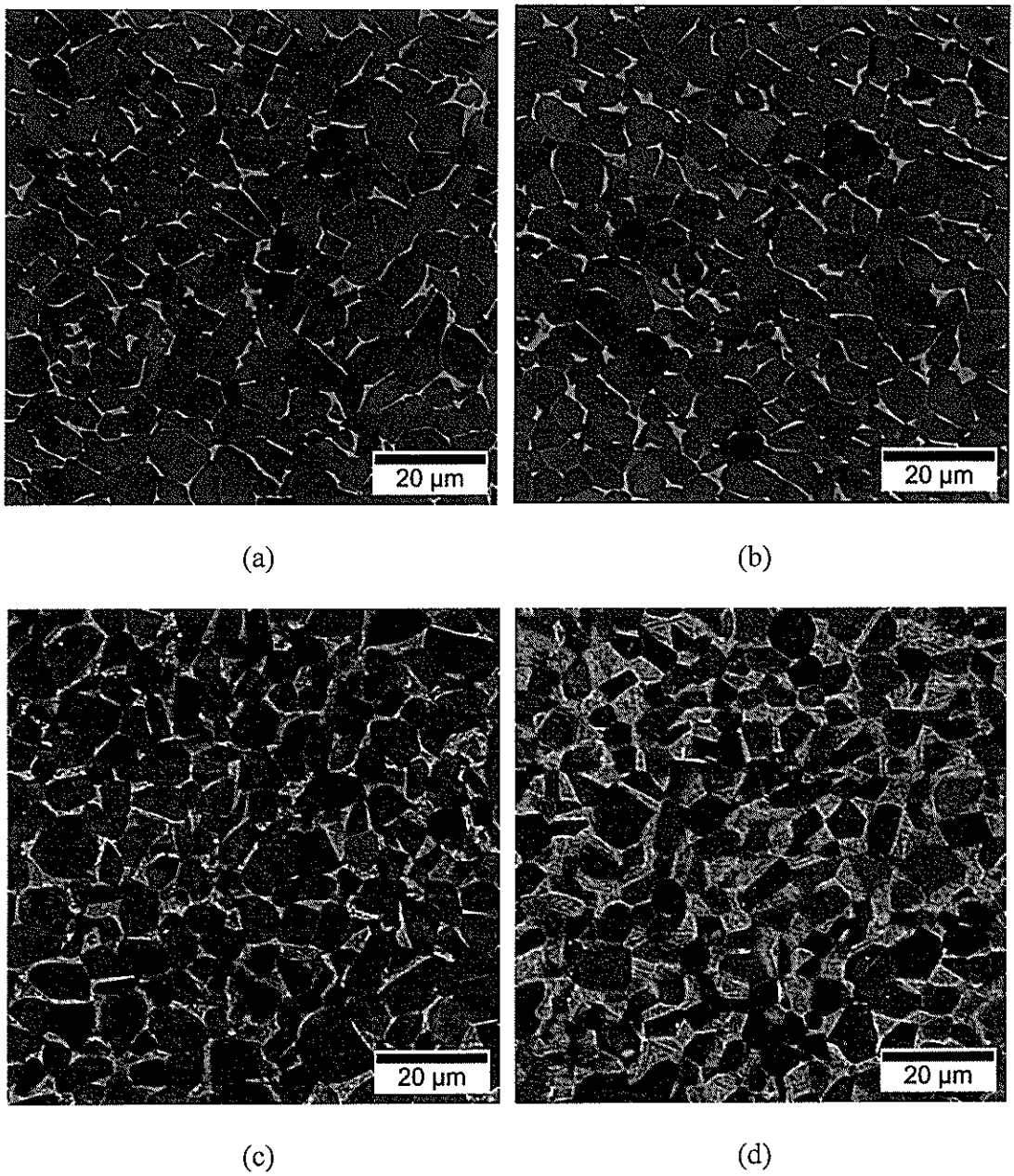

Fig. 3 BSE micrographs of CP Ti-6Al-4V (a) in the initial condition and just prior to SRJT or LRT at (b) 700 °C, (c) 800 °C, or (d) 900 °C. The dark and light areas denote the alpha and beta phases, respectively.

Kim *et al.* [18] suggested that alpha/beta interfaces play an important role in the activation of P/GBS in Ti-6Al-4V because these interfaces have lower resistance to sliding than alpha/alpha interfaces. The beta/beta interfaces were not considered here due to their small fraction and minor influence on P/GBS [19]. Thus, in the present study, analyses and discussions focused on both alpha particle and alpha grain structures.

4.2. High-temperature deformation behavior

4.2.1. Stress - strain rate relations

Log stress - log strain rate data from LRT (Fig. 4(a)) and SRJT (Fig. 4(b)) indicated increasing stress with increasing strain rate and decreasing temperature. The CP material exhibited higher stresses than the FP condition over the entire range of strain rate and temperature. However, the difference in flow stress between the CP and FP conditions was significantly decreased at high strain rates and 700°C for both LRT and SRJT. Kim *et al.* [13] reported a similar phenomenon in Ti-6Al-4V with a lamellar microstructure deformed at 715-900°C. According to this prior work, the flow stress of material with the thinnest alpha platelets was the lowest at low strain rates but the highest at strain rates over 10^{-3} s^{-1}. Such variations were explained on the basis of changes in the deformation mechanism at low and high strain rates. Such phenomena are discussed further for the present results in Section 5.2.

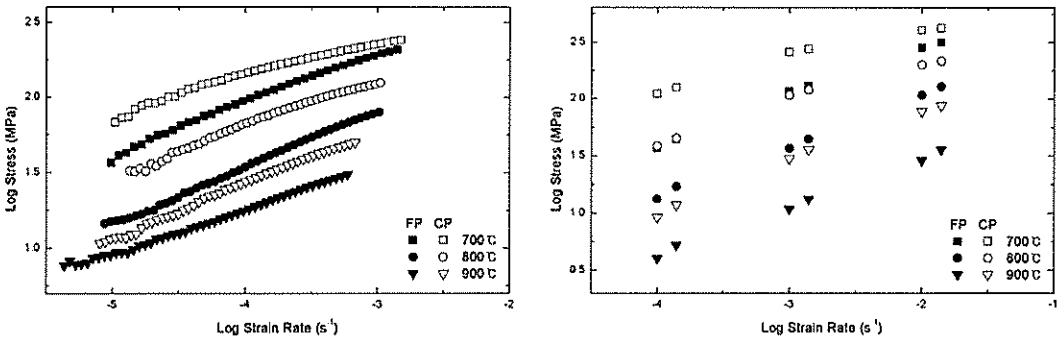

(a) (b)

Fig. 4 Log-log plot of stress - strain rate measurements at 700, 800, and 900 °C using an experimental approach based on (a) LRT (prestrain = 0.05) or (b) SRJT (prestrain = 0.25).

4.2.2. Strain rate sensitivity

SRJT results for the FP and CP conditions demonstrated that the strain rate sensitivity increased with decreasing particle size, decreasing strain rate, and increasing deformation temperature (Fig. 5). A similar tendency has been observed for Ti-6Al-4V with a transformed microstructure [20]. The present *m*-values appear reasonable in light of previous measurements based on the SRJT in the literature [9, 12, 14, 21]. Some researchers [13, 20] have reported somewhat lower *m*-values in comparison to the present data, which can be rationalized by the fact that these previous efforts utilized titanium alloys with a lamellar microstructure. The values calculated from LRT exhibited the same qualitative trends with respect to particle size, strain rate, and deformation temperature. However, these latter *m*-value results were consistently *smaller* for both FP and CP conditions (Fig. 6). This finding is also consistent with previous studies discussed in the Introduction.

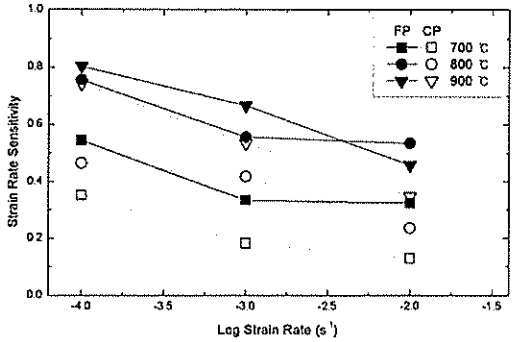

Fig. 5 Strain rate sensitivity of the FP and CP Ti-6Al-4V determined by SRJT (prestrain = 0.25) at various temperatures and strain rates.

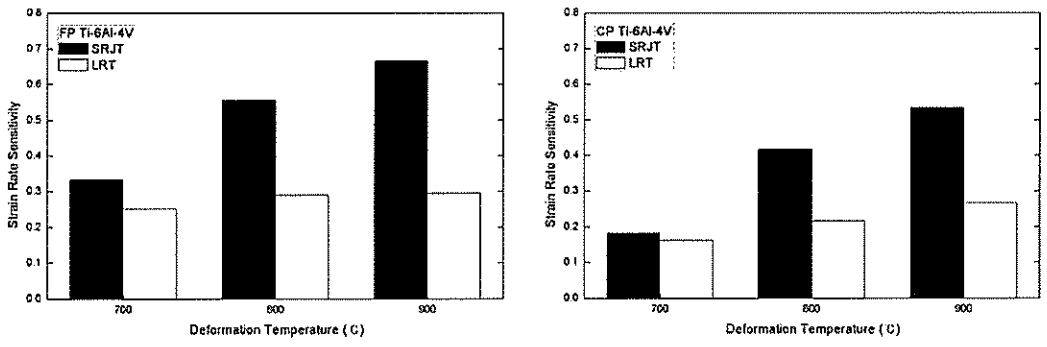

(a) (b)

Fig. 6 Comparison of the strain rate sensitivity from SRJT (prestrain = 0.25) and LRT (prestrain = 0.05) for Ti-6Al-4V in the (a) FP or (b) CP condition. The data were obtained at a strain rate of 10^{-3} s^{-1}.

4.3. Internal-variable analysis

LRT stress - strain rate results were fit based on the internal-variable analysis (Fig. 7) using constitutive parameters summarized in Table 1. The parameters $p = 0.15$ and $M_g = 0.5$ were determined from previous work using the internal-variable analysis of Ti-6Al-4V [22-24]. Both the internal stress for GMD (σ^*) and friction stress for P/GBS (Σ_g) decreased as

the deformation temperature increased. This phenomenon is attributed to the increasing fraction of the beta phase that exhibits a lower internal stress than the alpha phase and hence more readily accommodates stress concentrations developed at triple junctions [19].

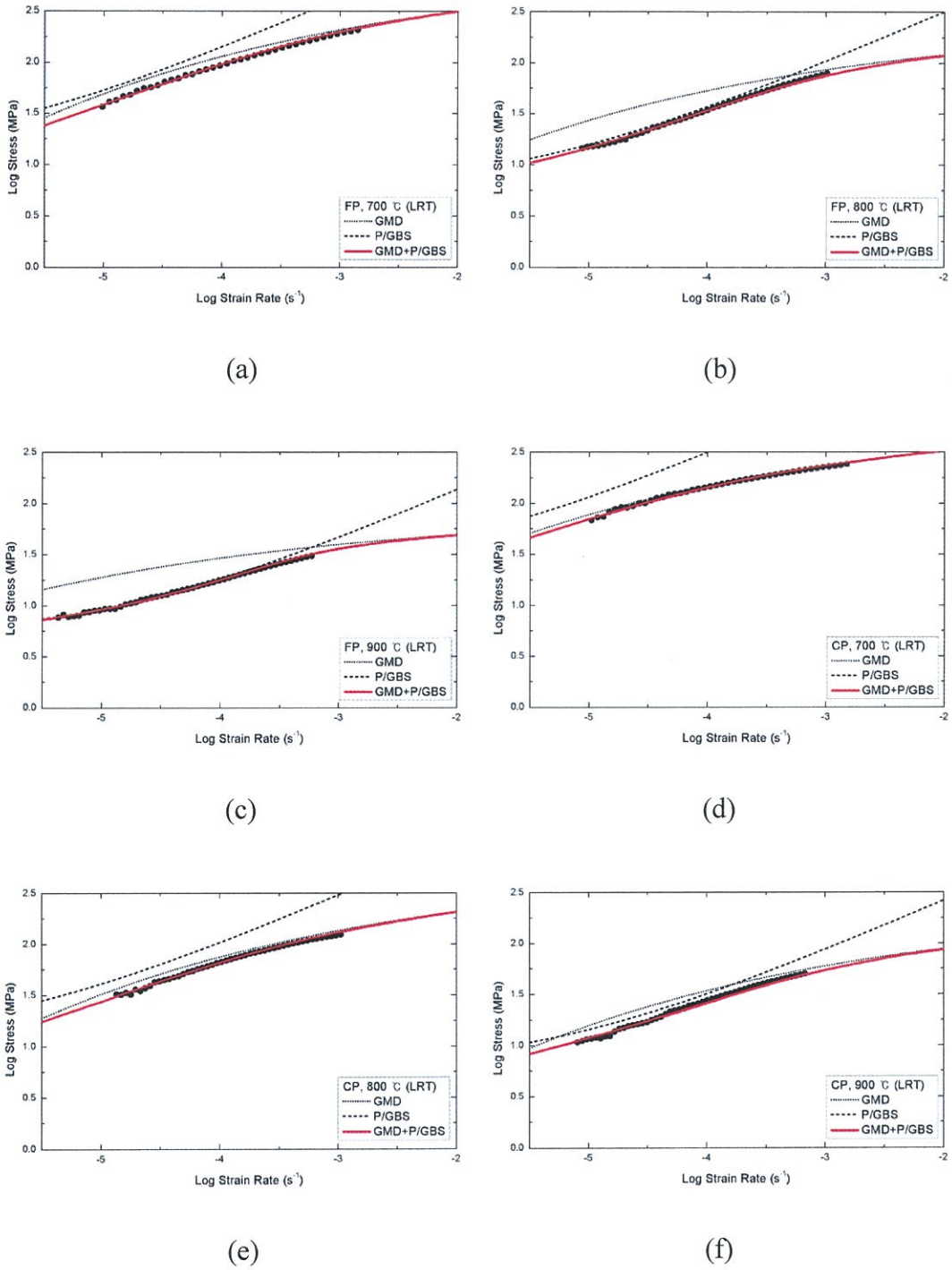

Fig. 7 Internal-variable analysis of LRT data (prestrain = 0.05) for Ti-6Al-4V in the (a-c) FP or (d-f) CP condition deformed at (a, d) 700 °C, (b, e) 800 °C, or (c, f) 900 °C.

Table 1. Constitutive parameters derived from the internal-variable analysis of LRT data

Sample	Temperature [°C]	GMD			P/GBS		
		$\log \sigma^*$	$\log \dot{a}^*$	p	$\log \Sigma_g$	$\log \dot{g}_o$	M_g
FP	700	2.91	-1.98	0.15	1.09	-6.05	0.5
	800	2.44	-2.57		0.77	-5.45	
	900	1.92	-3.87		0.71	-4.82	
CP	700	2.86	-2.67	0.15	1.36	-6.21	0.5
	800	2.76	-1.94		1.07	-5.79	
	900	2.36	-2.14		0.79	-5.24	

In Fig. 7, the stress - strain rate data fit well the GMD curve (Eq. (6)) for the limited range of strain rates higher than 10^{-3} s^{-1}, while deviations between the experimental data and this curve were found at lower strain rates. Thus, the P/GBS curve (Eq. (7)) was introduced to correct the deviations. As a result, all deformation behaviors were well described by a GMD+P/GBS curve, suggesting that both mechanisms operated during high-temperature deformation.

The present results may appear to contradict earlier work [13] which proposed that the deformation of Ti-6Al-4V could be explained totally by dislocation glide (*i.e.*, GMD) at 715 °C and 815°C. This work also suggested that the P/GBS strain rate (*i.e.*, $\dot{g}$ in Eq. (3)) was negligible even at 900°C. However, the earlier work focused on Ti-6Al-4V with a lamellar microstructure in which P/GBS is more difficult to activate than in an equiaxed structure [25]. Therefore, the present results that both mechanisms occur in all cases are reasonable due to the equiaxed nature of the program material. In the case of the FP Ti-6Al-4V deformed at 700°C, comprising both equiaxed and lamellar micro-constituents (Fig. 2(b)), the GMD curve is significantly closer to the experimental data compared with the other FP

conditions (Fig. 7(a)-(c)). This result also supports the present suggestion.

The SRJT results were also fit using the internal-variable theory (Fig. 8). GMD, P/GBS, and GMD+P/GBS curves were constructed using the parameters in Table 2. Compared to the LRT results (Fig. 7), the stress - strain rate plots from the SRJT experiments exhibited similar behavior such as the dependence of the constitutive parameters (*i.e.*, σ^* and Σ_g) on temperature, the preponderance of GMD at high strain rates, and the mixed control of GMD+P/GBS for the majority of entire range of strain rate. However, the two methods did exhibit differences in the specific contributions of the deformation mechanisms, as discussed further in Section 5.

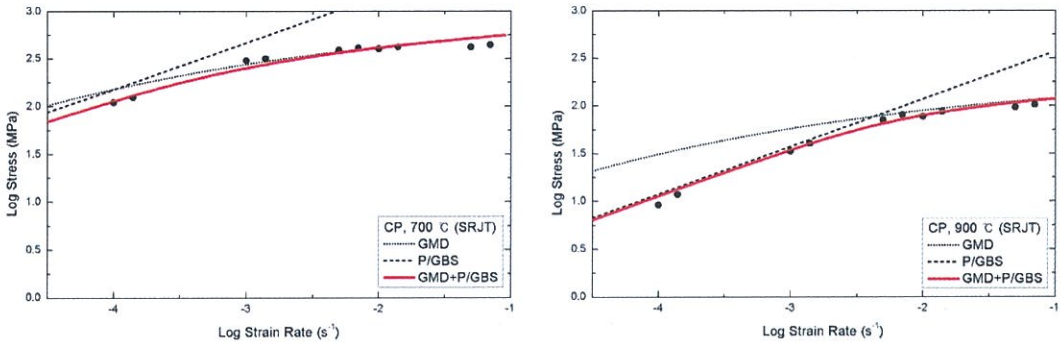

(a) (b)

Fig. 8 Internal-variable analysis of SRJT data (prestrain = 0.25) for Ti-6Al-4V in the CP condition deformed at (a) 700 °C and (b) 900 °C.

Table 2. Constitutive parameters derived from the internal-variable analysis of SRJT data

Sample	Temperature [°C]	GMD			P/GBS		
		$\log \sigma^*$	$\log \dot{a}^*$	p	$\log \Sigma_g$	$\log \dot{g}_o$	M_g
CP	700	3.07	-1.92	0.15	0.77	-6.78	0.5
	900	2.41	-1.83		-1.14	-8.42	

5. Discussion

5.1. Contribution of deformation mechanisms

The present work revealed that both GMD and P/GBS were activated under almost all test conditions. The relative contribution of each deformation mechanism was determined quantitatively from the LRT data at a strain rate of 10^{-3} s^{-1} (Fig. 9). Not surprisingly, the result demonstrated that the fraction of strain accommodated by P/GBS increased with increased fineness of microstructure and higher temperature. The FP sample deformed at 900°C exhibited the greatest fraction of P/GBS.

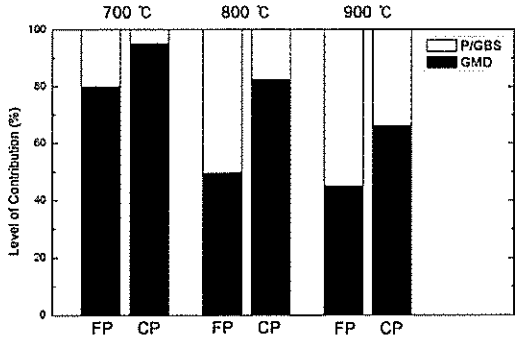

Fig. 9 Relative contributions of different deformation mechanisms to plastic flow determined by LRT (prestrain = 0.05) at a strain rate of 10^{-3} s^{-1}.

As shown in Section 4.3, the GMD curve well describes deformation behavior at high strain rates (Fig. 7 and Fig. 8), thus implying that GMD dominates in this regime. This trend can be found in other investigations using the internal-variable theory [13, 19, 23, 24] as well as research using a different theoretical method [21]. An analysis of the activation energy provided further insight into the possible cause for the predominance of GMD at high strain rates (Fig. 10). The apparent activation energy for deformation (Q) was estimated as

follows [26]:

$$Q = 2.303RS/m \tag{10a}$$

$$S = [\partial \log \sigma / \partial (1/T)] \tag{10b}$$

The activation energy at a strain rate of 10^{-3} s^{-1} was estimated to be 310 kJ mol^{-1} for the CP material and 294 kJ mol^{-1} for the FP material. These values are significantly higher than the activation energy for interphase/grain-boundary diffusion in Ti-6Al-4V (~189 kJ mol^{-1} [27]), suggesting the suppression of P/GBS accommodated by the boundary diffusion at this strain rate. The CP material deformed at a strain rate of 10^{-4} s^{-1} exhibited lower activation energy (247 kJ mol^{-1}), thereby suggesting that P/GBS related to boundary diffusion was activated to some extent. In addition, the activation energy of the FP material at this lower strain rate was estimated to be 204 kJ mol^{-1}, a value close to that for interphase/grain-boundary diffusion. Such a finding supports the conclusion that P/GBS predominates in a fine microstructure deformed at a low strain rate, as mentioned above.

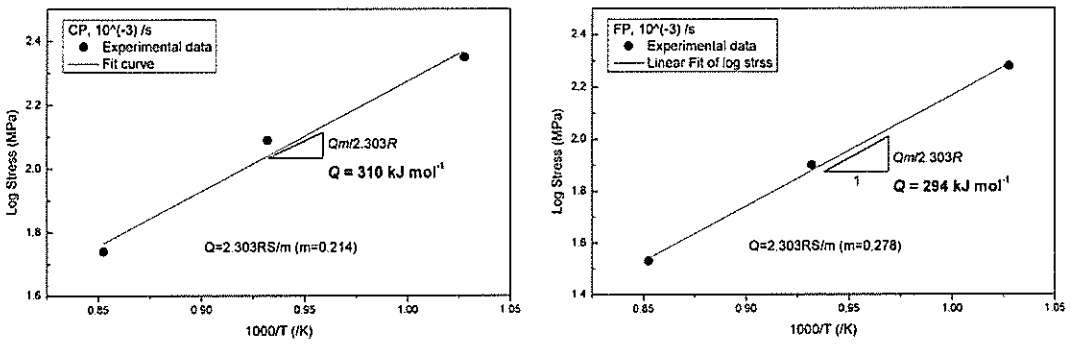

(a) (b)

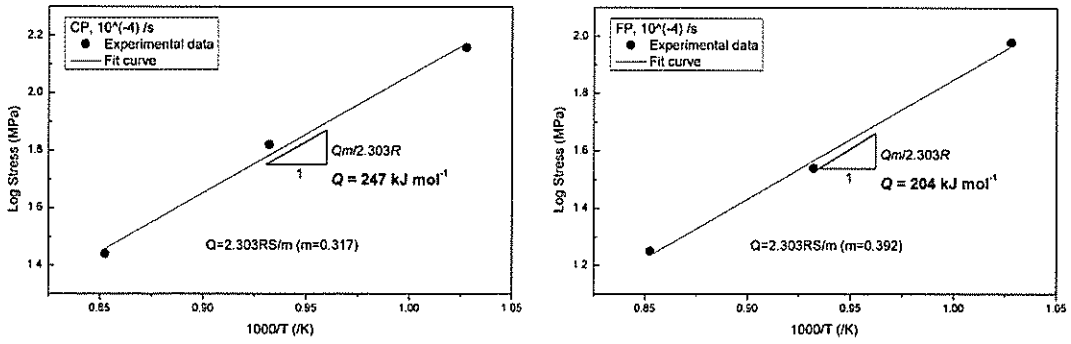

(c) (d)

Fig. 10 Dependence of flow stress on reciprocal temperature at (a, b) 10^{-3} s^{-1} and (c, d) 10^{-4} s^{-1} in (a, c) CP or (b, d) FP Ti-6Al-4V.

5.2. Peculiar flow behavior at 700°C

The high strain rate observations at 700°C revealed a considerably reduced difference in flow stress between the FP and CP conditions in both LRT and SRJT data (Fig. 4). Such trends can be rationalized in light of the fact that the contribution of P/GBS to plastic flow is decreased at high strain rates. Inasmuch as P/GBS is the primary factor for reducing the flow stress of fine-grained materials during high-temperature deformation [28, 29], the FP material maintained its high stress in the regime of suppressed P/GBS (*i.e.*, at high strain rates and low temperatures).

The contribution of Hall-Petch strengthening at smaller grain sizes may also play a role in the high-strain-rate / low-temperature results. In this respect, Semiatin and Bieler [20] suggested that a Hall-Petch-like effect can occur even at hot-working temperatures in a two-phase titanium alloy and is controlled largely by the alpha phase due to the limited number of slip systems in hcp structure. In the present work, the FP material contains a significant fraction of alpha (94.5%) at 700°C, presumably leading to Hall-Petch-like strengthening. In

contrast, such strengthening decreases rapidly at higher temperatures because of decreases in the fraction of alpha and the shear modulus.

5.3. Effect of experimental method on strain rate sensitivity

Irrespective of material condition (*i.e.*, FP or CP), the two different test methods used in the present work yielded different values of the strain rate sensitivity at a given strain rate and temperature. For example, the *m*-value of the CP material deformed at 900°C and 10^{-3} s^{-1} was 0.53 using the SRJT, but was only 0.27 per the LRT. The only exception to this general trend was noted for CP material deformed at 700°C and 10^{-3} s^{-1}, for which the strain rate sensitivities were comparable (~0.17) regardless of the test method (Fig. 6(b)). Hence, further investigation of the CP observations at 700°C and 900°C was undertaken to provide insight into the source of the different behaviors.

The strain rate sensitivity of a material is closely related to its deformation mechanisms. Indeed, a positive correlation was observed between the strain rate sensitivity and P/GBS contribution determined by the internal-variable analysis (Fig. 11), suggesting that the activation of P/GBS results in high *m*-values. The internal-variable analysis also revealed that a higher contribution of P/GBS to deformation in the SRJT samples compared to that in the LRT; the difference in the contribution between the two methods was considerably larger in the material deformed at 900°C (Fig. 12). Thus, the higher strain rate sensitivity of the SRJT material at 900°C can be attributed to its higher contribution of P/GBS in comparison to the corresponding LRT sample.

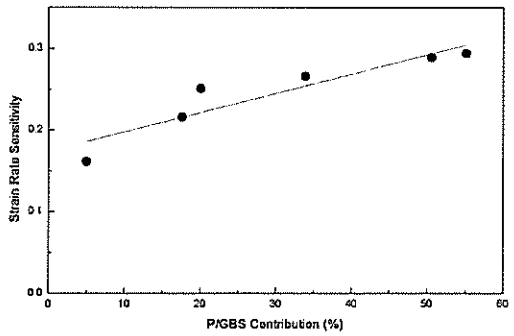

Fig. 11 Relationship between the strain rate sensitivity and P/GBS contribution based on data obtained from LRT (prestrain = 0.05) at a strain rate of 10^{-3} s^{-1}.

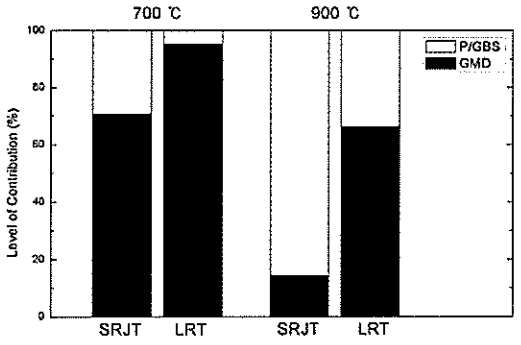

Fig. 12 Comparison of the relative deformations of different deformation mechanisms to plastic flow from internal-variable-model analysis of data from SRJT (prestrain = 0.25) and LRT (prestrain = 0.05) of Ti-6Al-4V in the CP condition deformed at a strain rate of 10^{-3} s^{-1}.

Microstructural factors determined from BSE and EBSD observations (Table 3) showed that the SRJT samples exhibited a larger particle size than the LRT materials. The difference in particle size between the two methods increased with increasing temperature. Such variations in particle diameter led to a 10% difference in the area per unit volume of the alpha/beta interfaces which are known to slide easily and control P/GBS and hence the magnitude of the strain rate sensitivity [18].

Table 3. Microstructural factors for the CP material deformed at 700°C and 900°C

Temperature [°C]	Method	D_α [μm]	$A_{\alpha/\beta}$	f_{HAGB}
700	LRT	7.08	1.00	0.74
	SRJT	7.27	1.04	0.76
900	LRT	7.19	1.18	0.81
	SRJT	7.50	1.29	0.71

**Dα: average diameter of alpha particles, Aα/β: relative area per unit volume of alpha/beta interfaces, fHAGB: fraction of high-angle grain boundaries*

In addition to variations in particle size, EBSD analysis revealed different grain structures (within individual alpha particles) that may have played a secondary role in the observed differences in strain rate sensitivity in the SRJT and LRT experiments (Fig. 13, Table 3). The CP materials deformed at 900°C exhibited a measurable difference in the fraction of high-angle grain boundaries, whereas samples deformed at 700°C had comparable values. In fact, the SRJT sample at 900°C exhibited regions consisting of as many as a dozen subgrains with low misorientations (Fig. 13(d)). Qi and Krajewski [30] studied the influence of the grain-boundary misorientation on GBS for aluminum using molecular dynamics simulations, and concluded that the misorientation exerted a strong effect on the amount of sliding along grain boundaries. In their work, each misorientation had a different grain-boundary energy, which exhibited a positive correlation with the GBS distance. Atomistic simulations performed by Namilae *et al.* [31] also suggested that an unstable material with a high grain-boundary energy showed substantial GBS. Therefore, it can be concluded that the difference in the nature of alpha-alpha boundaries in the SRJT and LRT samples for the CP condition deformed at 900°C may have affected the relative amounts of the P/GBS

contribution, whereas the similar grain structures in the samples at 700°C led to comparable contributions.

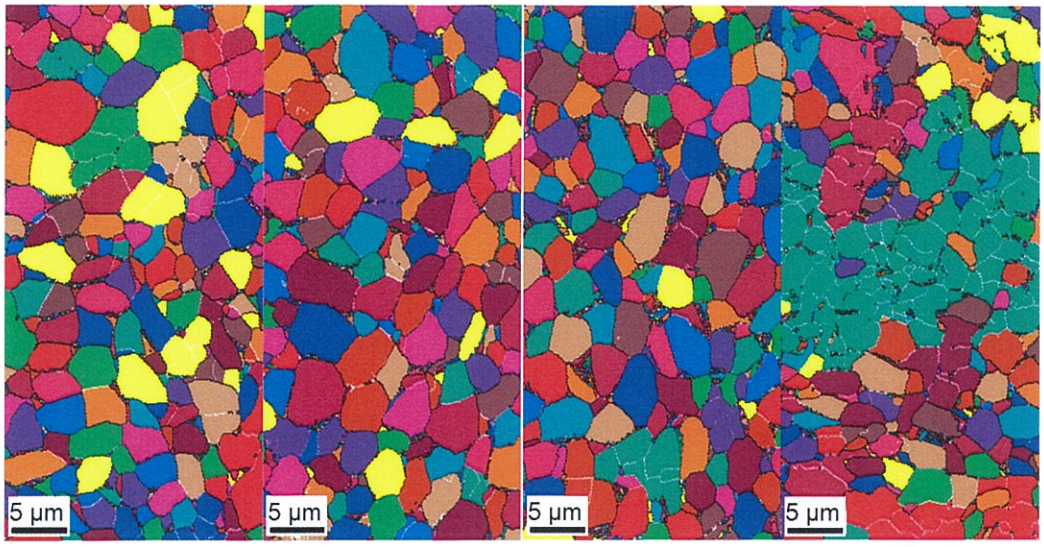

(a) (b) (c) (d)

Fig. 13 EBSD grain-ID maps for Ti-6Al-4V in the CP condition deformed via (a) LRT at 700 °C, (b) SRJT at 700 °C, (c) LRT at 900 °C, and (d) SRJT at 900 °C. Black and white lines indicate high-angle ($\theta > 15°$) and low-angle ($2° < \theta < 15°$) grain boundaries, respectively. The prestrain was 0.05 for the LRT and 0.25 for the SRJT.

5.4. Effect of prestrain

Hedworth and Stowell [11] and Booeshaghi and Garmestani [32] postulated that the larger plastic strain involved in the SRJT could change the microstructure. Their hypothesis can be interpreted in light of the variations in particle and grain structures described in Section 5.3. Indeed, the present work used different prestrains and prestrain rates for the two methods as mentioned in Section 3. The imposed conditions were those typically employed in other research described in the literature [16, 23, 24]. Nevertheless, additional LRT

experiments were conducted on a CP sample at 900°C to elucidate the specific effect of prestrain on microstructure. For the comparison, average *m*-values for each level of prestrain were calculated in a strain-rate range of $10^{-4} < \dot{\varepsilon} < 10^{-3}$ s^{-1} in which the data reflected the microstructural differences demonstrated in Table 3. The results revealed that an increase in prestrain prior to LRT yielded substantially higher *m*-values (Fig. 14). In particular, the *m*-value determined with the same prestrain as in the SRJT (*i.e.*, 0.25) was significantly higher than that determined at lower prestrains and was indeed comparable to the SRJT value. Thus, it is reasonable to conclude that the prestrain affected the microstructure and the corresponding P/GBS contribution to deformation behavior.

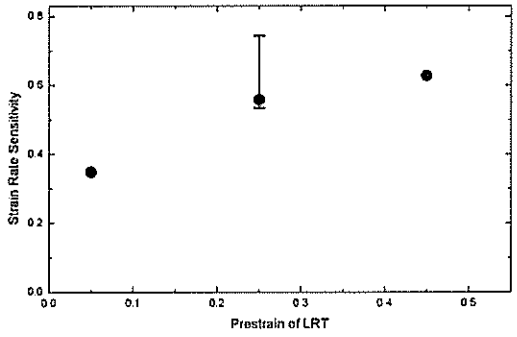

Fig. 14 Dependence on prestrain of the strain rate sensitivity determined from LRT on CP Ti-6Al-4V deformed at 900 °C in the strain-rate range of $10^{-4} < \dot{\varepsilon} < 10^{-3}$ s^{-1}. The scatter band at a prestrain of 0.25 denotes the range of m-values determined by SRJT for CP Ti-6Al-4V deformed at 900 °C between strain rates of 10^{-4} s^{-1} and 10^{-3} s^{-1}.

6. Conclusions

Quantitative analysis based on the internal-variable theory was performed for the FP and CP Ti-6Al-4V which had been deformed at 700, 800, and 900°C via the SRJT and LRT methods. The results were compared with each other to elucidate the source of differences in the strain rate sensitivity depending on the test method. The following conclusions were drawn:

Fitted GMD+P/GBS curves from the internal-variable analysis were in good accord with the stress - strain rate data in all cases, suggesting that both mechanisms operate during high-temperature deformation. The GMD curves fit the experimental data only at high strain rates due to the suppression of P/GBS in this range. P/GBS contributes more to the total deformation in the finer microstructure, higher temperature, and lower strain rate instances. Both internal and friction stresses determined from the internal-variable theory decrease with increasing temperature due to the increasing fraction of the beta phase.

The CP Ti-6Al-4V exhibits generally higher flow stress than the FP Ti-6Al-4V at a given strain rate and temperature. However, the difference in flow stress between the CP and FP materials is significantly reduced at high strain rates and 700°C for both SRJT and LRT. Such a behavior is attributed to the different deformation mechanisms at low and high strain rates as well as possible contributions to the flow stress from the Hall-Petch-like effect at temperatures at which the volume fraction of the second phase (*i.e.*, beta phase) is very small.

The strain rate sensitivities obtained in the present work are reasonable in view of earlier results. However, clear differences in the strain rate sensitivity are observed depending on the experimental method used to determine it. The strain rate sensitivity determined by the SRJT is consistently higher than that from the LRT, in broad agreement with previous observations for Ti-6Al-4V as well as other materials. This discrepancy can be attributed to

the different contribution of P/GBS between the two methods. The SRJT samples exhibit the higher P/GBS contribution compared with the LRT materials due to differences in both alpha particle and grain structures. The higher fraction of alpha/beta interfaces in the SRJT samples induces a decreased resistance to P/GBS and hence yields high strain rate sensitivity. The considerable difference in the alpha-grain-boundary misorientation between the SRJT and LRT samples could exert a secondary influence on the disparity in the P/GBS contribution. The effect of prestrain on microstructure evolution must be taken into account when interpreting the flow behavior from the two test methods.

References

[1] F.J. Zerilli, R.W. Armstrong, *Journal of Applied Physics* 61 (1987) 1816-1825.

[2] T.K. Ha, Y.W. Chang, *Acta Materialia* 46 (1998) 2741-2749.

[3] S.B. Brown, K.H. Kim, L. Anand, *International Journal of Plasticity* 5 (1989) 95-130.

[4] H.J. McQueen, N.D. Ryan, *Materials Science and Engineering A* 322 (2002) 43-63.

[5] S.L. Semiatin, F. Montheillet, G. Shen, J.J. Jonas, *Metallurgical and Materials Transactions A* 33 (2002) 2719-2727.

[6] R.C. Picu, A. Majorell, *Materials Science and Engineering A* 326 (2002) 306-316.

[7] J. Cai, F. Li, T. Liu, B. Chen, M. He, *Materials & Design* 32 (2011) 1144-1151.

[8] M.J. Stewart, *Metallurgical and Materials Transactions A* 7 (1976) 399-406.

[9] C.H. Hamilton, A.K. Ghosh, *Metallurgical and Materials Transactions A* 11 (1980) 1494-1496.

[10] D. Lee, E. Hart, *Metallurgical and Materials Transactions B* 2 (1971) 1245-1248.

[11] J. Hedworth, M.J. Stowell, *Journal of Materials Science* 6 (1971) 1061-1069.

[12] S.L. Semiatin, P.N. Fagin, J.F. Betten, A.P. Zane, A.K. Ghosh, G.A. Sargent, *Metallurgical and Materials Transactions A* 41 (2010) 499-512.

[13] J.H. Kim, S.L. Semiatin, C.S. Lee, *Acta Materialia* 51 (2003) 5613-5626.

[14] G.A. Sargent, A.P. Zane, P.N. Fagin, A.K. Ghosh, S.L. Semiatin, *Metallurgical and Materials Transactions A* 39 (2008) 2949-2964.

[15] A.K. Ghosh, C.H. Hamilton, *Metallurgical and Materials Transactions A* 10(1979) 699-706.

[16] C.H. Park, B. Lee, S.L. Semiatin, C.S. Lee, *Materials Science and Engineering A* 527 (2010) 5203-5211.

[17] T. Lee, C.H. Park, D.-L. Lee, C.S. Lee, *Materials Science and Engineering A* 528 (2011)

6558-6564.

[18] J.S. Kim, J.H. Kim, Y.T. Lee, C.G. Park, C.S. Lee, *Materials Science and Engineering A* 263 (1999) 272-280.

[19] J.H. Kim, S.L. Semiatin, C.S. Lee, *Materials Science and Engineering A* 394 (2005) 366-375.

[20] S.L. Semiatin, T.R. Bieler, *Acta Materialia* 49 (2001) 3565-3573.

[21] S.L. Semiatin, M.W. Corbett, P.N. Fagin, G.A. Salishchev, C.S. Lee, *Metallurgical and Materials Transactions A* 37 (2006) 1125-1136.

[22] J.S. Kim, Y.W. Chang, C.S. Lee, *Metallurgical and Materials Transactions A* 29 (1998) 217-226.

[23] Y.G. Ko, W.G. Kim, C.S. Lee, D.H. Shin, *Materials Science and Engineering A* 410-411 (2005) 156-159.

[24] Y.G. Ko, C.S. Lee, D.H. Shin, S.L. Semiatin, *Metallurgical and Materials Transactions A* 37 (2006) 381-391.

[25] J.S. Kim, K. Kibble, M. Stanford, *Materials Science and Engineering A* 532 (2012) 236-244.

[26] V. Seetharaman, S.L. Semiatin, *Metallurgical and Materials Transactions A* 28 (1997) 2309-2321.

[27] A. Arieli, A. Rosen, *Metallurgical and Materials Transactions A* 8 (1977) 1591-1596.

[28] K. Maruyama, Y. Wananabe, H. Oikawa, *Acta Metallurgica* 34 (1986) 2343-2351.

[29] H. Oikawa, K. Sasaki, A. Sagara, K. Maruyama, *Journal of Materials Science Letters* 7 (1988) 987-988.

[30] Y. Qi, P.E. Krajewski, *Acta Materialia* 55 (2007) 1555-1563.

[31] S. Namilae, N. Chandra, T.G. Nieh, *Scripta Materialia* 46 (2002) 49-54.

[32] F. Booeshaghi, H. Garmestani, *Scripta Materialia* 40 (1999) 509-516.

Appendix

The present results were submitted to Acta Materialia on August 12, 2012. The submitted manuscript was attached in the following pages.